Canadian Science Publishing | Canadian Geotechnical Journal

Effects of foundation pressure and building stiffness on tunnel-separated footing interaction

Journal:	*Canadian Geotechnical Journal*
Manuscript ID	cgj-2024-0744.R2
Manuscript Type:	Research Article
Date Submitted by the Author:	08-Mar-2025
Complete List of Authors:	Xu, Jingmin; Southeast University, Underground Engineering; University of Cambridge, Department of Engineering Wang, Yukun; Southeast University, Underground Engineering Gao, Ming; Southeast University, Underground Engineering Ni, Jun-Jun; Southeast University Cao, Liqiang; Beijing University of Technology, College of Architecture and Civil Engineering
Is the manuscript for consideration in a Special Issue or Collection?:	Not applicable (regular submission)
Keyword:	Tunnels & Tunneling, Soil/structure interaction, Separated footings, Shear distortion, Numerical modeling

Effects of foundation pressure and building stiffness on tunnel-separated footing interaction

Jingmin Xu[a,b], Yukun Wang[a], Ming Gao[a], Jun-jun Ni[a], Liqiang Cao[c*]

[a] School of Transportation, Southeast University, Nanjing 211189, China.

[b] Department of Engineering, University of Cambridge, Cambridge CB2 1TN, UK

[c] Institute of Geotechnical and Underground Engineering, Beijing University of Technology, Beijing 100124, China

*Corresponding author Email: lqcao@bjut.edu.cn (Liqiang Cao)

Abstract

The displacements and deformations of buildings with separated footings caused by tunneling may be significant and could damage the structures. This paper numerically investigates the influences of building stiffness, geometry and foundation pressure on the deformation of a two-story elastic framed building due to tunneling in sand. An advanced soil constitutive model known as hypoplastic model was calibrated and adopted to simulate the sand behavior. Results show that the roles of building stiffness and foundation pressure on the footing displacements due to tunneling are significant, particularly for a larger tunnel volume loss. An increase in building stiffness reduces both the vertical and horizontal displacements of footings, while a greater foundation pressure primarily increases footing settlements. The influences of building stiffness and foundation pressure on building shear distortion are considerable, while their impacts on panel horizontal strains are minor for the investigated parameter ranges. The results also suggest the potential use of greenfield results as a conservative estimation of the distortion of buildings with separated, embedded footings when subjected to tunneling-induced displacements. Modification factors for shear distortion and horizontal strains are presented and show good agreement with the empirical centrifuge-derived envelopes for buildings resting on the soil surface.

Keywords: Tunnels & Tunneling; Soil/structure interaction; Separated footings; Shear distortion; Horizontal strain; Numerical modeling

Notation list

b_f	footing width	$M^{\varepsilon,h}$	horizontal strain modification factor
B	building transverse width	n	exponent for hypoplastic model
C	cover depth	S	slope
D_{50}	sand average diameter	U_x	horizontal displacement
D	tunnel diameter	U_z	settlement
e	horizontal distance	$V_{l,t}$	tunnel volume loss
e_{c0}	maximum void ratio at zero pressure	w	tilt
e_{d0}	minimum void ratio at zero pressure	w_p	width of the panel
e_{i0}	critical void ratio at zero pressure	z_t	tunnel axis depth
e_{max}	maximum void ratio of sand	α	exponent for hypoplastic model
e_{min}	minimum void ratio of sand	α_f^*	relative footing-soil stiffness per metre run
E_s	representative stiffness of the soil	β	shear distortion
E	Young's modulus	φ'_c	critical state friction angle
$\overline{GS}_{max}$	maximum greenfield slope, defined as the maximum slope of a movable, a bay width-long line segment on the greenfield settlement curve.	γ	exponent for hypoplastic model
GA_s^*	building shear stiffness per metre run	ε_h	horizontal strain
h_f	height of the footing column	ε_d	diagonal strain
h_s	granular hardness	ε_{max}	maximum tensile strain
I_d	relative density of sand	$\varepsilon_{max,gf}$	maximum average horizontal strains of greenfield displacements within a bay width
K_b, K_c	average stiffness of the beam, column	κ	soil-building shear stiffness
K_0	coefficient of horizontal pressure	ρ_s	soil density
M^{β}	shear distortion modification factor	ρ	density of building materials

1 Introduction

With rapid population growth and the increasing complexity of infrastructure systems, underground construction has become essential, particularly for expanding transportation networks in densely populated urban areas. While tunneling offers a practical solution for developing new infrastructure, it inevitably induces ground movements that can threaten the stability of nearby structures (Mair et al. 1996; Ng et al. 2022; Shi et al. 2022). As urban environments become increasingly crowded, predicting and mitigating these tunneling-induced movements is crucial to ensuring the safety of both new and existing buildings.

A widely adopted method for evaluating building distortion caused by tunneling is the multi-stage assessment framework introduced by Mair et al. (1996). In the initial stage, predictions are made regarding the greenfield surface settlements induced by tunneling. The second stage then assesses potential building damage by assuming that the structure deforms in accordance with these predicted greenfield displacements. To provide a more accurate evaluation in the third stage, soil-structure interaction is accounted for. This refinement can be achieved through comprehensive modeling of the entire tunnel-soil-building system (Maleki et al. 2011; Boldini et al. 2018; Ritter et al. 2018; Franza and DeJong, 2019; Miliziano et al. 2022; Yu et al. 2022; Xu et al, 2024) or by using empirical modification factors based on the relative stiffness of the building and the soil (Potts and Addenbrooke, 1997; Franzius et al. 2004; Xu et al. 2020, 2021b; Franza et al. 2022; Yu et al. 2025). For instance, a modification factor for building shear distortion was proposed based on the centrifuge results and subsequently linked to the relative soil-building shear stiffness parameter (Xu et al. 2020, 2021b), providing useful guidance for the quick assessment of structural distortion in tunneling projects. Typically, in both numerical models and centrifuge tests, buildings are frequently simplified

as equivalent beams or plates for these evaluations (Pickhaver et al. 2010; Maleki et al. 2011; Franza et al. 2022). Recent studies have emphasized the critical need to account for structural details when addressing tunnel-building interaction issues, highlighting the shortcomings of using the equivalent solid method (Ritter et al. 2018; Boldini et al. 2018; Xu et al. 2020). These limitations are particularly evident for buildings with low shear stiffness, unless a Timoshenko beam, which incorporates shear flexibility, is employed (Franza et al. 2020).

To assess the degree of distortion in buildings subject to differential settlements induced by tunneling, various deformation parameters are commonly employed, such as deflection ratio (Potts and Addenbrooke, 1997), axial strain (Elkayam and Klar, 2019), and shear/angular distortion (Son and Cording, 2005). The dominant mode of deformation in a building is determined by its bending-to-shear stiffness ratio (Burland et al. 1977). Short masonry or framed structures generally undergo shear distortion, whereas longer masonry buildings tend to experience bending-dominated deformation. Additionally, buildings with discontinuous foundations are particularly affected by tunneling-induced soil horizontal displacements. Goh and Mair (2014) simulated framed buildings on both continuous and discontinuous footings adjacent to a multi-propped excavation, finding that horizontal strains were negligible for continuous footings but significant for structures with separated footings, with the maximum strain locations differing from those in the greenfield. Franza and DeJong (2019) also reported significant horizontal displacements and strains in buildings with separated footings, highlighting the complexity of soil-footing interactions, which are influenced by both the stiffness and height of footing columns. Although recent centrifuge experiments (Xu et al. 2021a, b) provide experimental evidence of the horizontal responses of separated footings to tunneling, manufacturing issues in these studies introduce uncertainties in the accurate quantification of

horizontal displacements and strains.

In summary, while researchers have recognized the significance of addressing horizontal deformation in buildings with discontinuous foundations, such as separated footings, the complex interaction mechanisms between soil and these footings, especially when considering various structural and tunneling-related factors, remain insufficiently explored. Recent centrifuge studies (Xu et al. 2020, 2021a, b) have demonstrated that buildings with higher foundation pressure (i.e., building weight) or lower stiffness are more prone to greater distortion. However, the effects of these factors on the horizontal behavior of footings remain unclear, highlighting the need for further research to ensure accurate predictions of horizontal strains and potential damage to buildings in tunneling projects.

This paper fills the existing research gap by presenting a numerical analysis of the response of framed buildings with separated footings to tunnel excavation in sandy soils. The focus lies on how foundation pressure and building stiffness influence the interaction between tunnels and framed structures. Furthermore, the study examines the effects of various parameters, including the building's transverse width, its eccentricity from the tunnel axis, and the cover depth of the tunnel, on ground deformation and building distortion due to tunneling. The study begins with an analysis of ground surface and footing displacements resulting from tunnel excavation, followed by an investigation of subsurface soil movements influenced by the surface frames with separated footings. To assess structural damage, the analysis includes calculations of angular distortion and horizontal strain at the ground level, serving as a base for damage classification. Ultimately, the study presents modification factors for angular distortion and horizontal strain, linking them to the relative stiffness of both the soil and building. These insights are crucial for evaluating the risk of tunneling-induced damage to

structures.

2 Finite element model

2.1 Problem definition

The scenario studied in this paper, illustrated in Figure 1, involves the construction of a 6.12 m diameter D tunnel beneath a framed building with separated footings in dry sand. The tunnel is positioned at two different cover depths (C) of 7.96 m (cover-to-diameter ratio C/D=1.3) and 12.24 m (C/D=2.0), resulting in tunnel axis depths (z_t) of 11.02 m and 15.3 m, respectively. These dimensions align with centrifuge experiments from Xu et al. (2021b), enabling direct comparison between the numerical simulations and experimental data (68 times the gravity level) for a full-scale (prototype) scenario.

The framed building used in the models has a footing embedment depth of 1.0 m, story height of 2.6 m, and a transverse width (B) of either 31.3 m (long) or 15.8 m (short). The building's eccentricity (e/B) is 0 for long frames and 0.5 for short frames, where e represents the horizontal distance between the tunnel and the building's center. Each building element has a uniform thickness of 0.22 m, and the frame panel width (w_p) is set to 5.2 m. Variations in building stiffness and footing pressure were introduced by adjusting the material's Young's modulus (E = 30, 50, 70 GPa) and density (ρ = 1600, 2700, 3800, 4900 kg/m^3), respectively. The footing width, b_f, varies from 0.68 m to 1.09 m in some models, as it also influences the pressure beneath the footing. As outlined in Table 1, 25 numerical models were analyzed, including two greenfield models and 23 tunnel-soil-frame interaction models, which were grouped into six categories based on specific parameters.

2.2 Element mesh and boundary conditions

In this study, ABAQUS finite element (FE) software (Hibbitt, 2002) was used to analyze the

interaction between tunneling and separated footings. A mesh sensitivity analysis guided the creation of the FE mesh for both the soil and the framed structure, ensuring that a further increase in the number of elements had a negligible influence on the FE modeling results, as illustrated in Figure 2. The model dimensions were 43.5 m wide (7.1*D*) and 16.1 m deep (2.6*D*); this is consistent with the centrifuge model size, and the numerical sensitivity analysis results show that further increasing the model dimensions has a negligible influence on the results (Supplemental Material). Eight-node plane strain elements (CPE8) were employed to simulate the soil, framed building, and tunnel lining. Boundary conditions included fixing the soil at the bottom, while lateral nodes were restrained vertically. No constraints were imposed on the structure or soil surface.

Note that the plane-strain models adopted in this paper indicate continuous walls of the building in the out-of-plane direction. For a real framed building, the walls are usually discontinuous due to the presence of openings. Therefore, the plane-strain building model may overestimate the building stiffness and thus underestimate the structural response to tunnel construction. The scenario of a three-dimensional building affected by the tunnel excavation process is the closest to real engineering conditions. However, this is out of the scope of this paper.

2.3 Constitutive model and model parameters

Von Wolffersdorff (1996) developed the hypoplastic model, which integrates pressure and density dependencies to accurately predict sand behavior, including volumetric changes from shearing and stiffness degradation at small strains (Herle and Gudehus, 1999). This model has been widely utilized in complex soil-structure interaction studies, providing reliable data (Khalajzadeh et al. 2023; Song et al. 2023; Xu et al. 2024 a,b). It comprises eight parameters: critical state friction angle (φ'_c), granular hardness (h_s), a fitting parameter (n), minimum, maximum, and critical void ratios at zero

pressure (e_{d0}, e_{i0}, e_{c0}), and α and γ, which govern the volumetric behavior and the nonlinear stress-strain response of the soil. The calibration of these parameters is based on oedometer and drained triaxial compression test data, as detailed in Song and Marshall (2020).

To compare with the centrifuge test data from Xu et al. (2021b), the same fine-grained silica sand, 'Leighton Buzzard Fraction E,' was modeled with a relative density (I_d) of 90%, resulting in a density (ρ_s) of 1603 kg/m³. This sand has a mean diameter of D_{50} = 0.14 mm, with maximum (e_{max}) and minimum (e_{min}) void ratios of 1.01 and 0.61, respectively (Zhao, 2008; Lanzano et al. 2016). The soil constructive parameters are summarized in Table 2. The tunnel lining was modeled as a linear elastic material with an unrealistically high Young's modulus of 21,000 GPa to ensure reliable control of displacements at the tunnel boundary. The interfaces between soil and structures (footings and the tunnel) were simulated using the Coulomb friction law, with a friction coefficient of tan(φ'_c) = 0.62, indicative of a rough soil-structure interface (Song and Marshall, 2020).

2.4 Numerical modeling procedure

The tunnel construction simulation employs a displacement-controlled method, using tunnel volume loss as the input parameter. To represent the displacements associated with shallow tunnels, a homothetic contraction of the tunnel cross-section is centered on the fixed tunnel invert, as illustrated in Figure 2 (Cheng et al. 2007). This is achieved by prescribing boundary displacements that are proportional to the target tunnel volume loss $V_{l,t}$. The procedures for the finite element analysis simulation can be outlined as follows. Initially, a geostatic step was performed to establish a predefined stress distribution (lateral earth pressure coefficient K_0=0.5) within the soil elements. Subsequently, soil elements within the tunnel and footings are removed, allowing for the activation of the tunnel lining, framed buildings, and soil-structure interfaces. Finally, a non-uniform

displacement profile is applied to the tunnel boundary elements to replicate the tunnel excavation. This displacement-control method has been widely employed in both centrifuge testing (Boonsiri and Takemura, 2015) and numerical modeling (Boldini et al. 2021; Xu et al. 2024).

2.5 Numerical model validation

To verify the current numerical modeling methodology, the study compares tunneling-induced surface soil displacements in greenfield conditions, displacements of separated footings, and movements of the underlying soil, all corresponding to a tunnel volume loss of $V_{l,t}$=1.0%. This value of $V_{l,t}$ was chosen because, in practical projects of closed face tunneling in soft soil (particularly in sand), a high settlement control degree is usually achieved, resulting in a low tunnel volume loss of 0.5~1.0% (Mair and Taylor, 1999). This comparison is illustrated in Figure 3, utilizing data from both the numerical analysis presented in this paper and centrifuge models reported by Xu et al. (2021b). In this paper, downward and rightward displacements are defined as positive, with U_x and U_z representing horizontal and vertical displacements, respectively. Also, note that near-surface movements were compared because they are more important in investigating the response of buildings with shallow foundations to tunnel construction.

Figures 3(a) and (b) indicate that the settlement trough induced by tunneling in greenfield conditions is slightly wider and shallower in the finite element (FE) models compared to the centrifuge results. This variation may arise from differences in the modeling approaches used for tunnel volume loss. Research by Song and Marshall (2020) has demonstrated that the settlement trough associated with displacement-controlled tunneling (as reported in this study) is wider and shallower than that resulting from pressure-controlled tunneling (Xu et al. 2021b). However, various studies (Ng et al. 2012; Giardina et al. 2015; Boldini et al. 2021) have also reported that the numerical

models tend to produce wider and shallower surface settlements than those observed experimentally or in the field. In terms of horizontal soil displacements, the numerical findings closely align with the magnitude of the centrifuge data, suggesting that the numerical model accurately replicates the realistic displacements of sandy ground during tunneling in greenfield conditions.

Additionally, the agreement between the numerical and centrifuge results regarding footing settlements and horizontal displacements is generally good, with the numerical model predicting smaller settlements and larger horizontal displacements. This discrepancy may be attributed to the different greenfield displacements obtained from the two methods. However, it was found that the use of square aluminum bars in the panel corners to secure the columns and beams of the frame models in the centrifuge tests conducted by Xu et al. (2021b) also affected the results. On one hand, the square aluminum bars contributed to increased building weight by ~10.0%, which resulted in larger footing settlements. This manufacturing technique in the centrifuge tests also resulted in a lower (reduced by ~14.9%) total stiffness of the building, which further caused a more flexible building response to tunneling. On the other hand, these square aluminum bars also shortened the effective length (by ~13.1%) of the footing columns, leading to a stiffer response in the horizontal direction to tunneling. Consequently, horizontal displacements of strip footings in the centrifuge tests were somewhat smaller than those predicted by the finite element (FE) model.

Furthermore, footing penetration depth after tunneling in the FE model is consistently smaller than that observed in the centrifuge tests. This finding aligns with Boldini et al. (2021), who reported similar numerical simulations with the SANISand constitutive model, that the numerical models tend to underestimate footing penetration. This result highlights a limitation in the current soil constitutive models, both in this study and Boldini et al. (2021), in fully capturing the actual footing penetration

depth. However, the overall interaction mechanism between the tunnel and buildings with separated footings is well-replicated by the numerical model, approving its reliability and supporting its application in further investigations.

3 Results

In this section, results for a tunnel volume loss of $V_{l,t}$=2.0% are presented, unless otherwise stated. This level of tunnel volume loss was chosen because the worst-case scenario is often considered in urban tunneling projects for design purposes.

3.1 Effects of foundation pressure

The effects of foundation pressure (building load) on the response of framed buildings with separated footings to tunneling are discussed using the data presented in Figures 4 and 5. First, the response of the long central frames to tunnel construction is considered. Figure 4(a) shows that an increase in foundation pressure increases the maximum settlement of the central footings, while its effect on the external footings (foot-1 and foot-7) is negligible. Consequently, greater differential settlements between footings are observed for the buildings with a larger foundation pressure. For the building with the greatest foundation pressure, the footings tend to settle following the greenfield displacement, suggesting a flexible response of buildings to tunneling.

In terms of horizontal displacements, the building footings in all models generally follow the greenfield displacements but exhibit slightly smaller movements, with foundation pressure having a negligible effect on the results. This suggests that there is no slippage at the interface between the base of the footing and underlying soil, regardless of the foundation pressure (see Figure 4(c)). Finally, it is found that the above conclusions can be also applicable to the cases with deeper tunnels (see

Figure 4(d)); only the magnitude and distribution of the displacements (both the footings and underlying soil) show a slight difference for different tunnel depths.

The influence of foundation pressure on the response of short eccentric frames to tunneling is now considered. Unlike the long central frame, Figures 5(a) and 5(b) show that all footings in the short eccentric frame experience greater settlements as foundation pressure increase. In this case, the increased foundation pressure may not result in a greater building deformation (discussed later in this paper). On the other hand, the footings for short eccentric frames display slightly larger horizontal displacements than greenfield displacements, and the larger the foundation pressure, the greater the horizontal displacements. Furthermore, the role of foundation pressure in the horizontal response of footings to tunnel construction is less significant for a deeper tunnel case (compare Figure 5(c) with Figure 5(d)).

Note that this paper did not consider the symmetric cases of short frames because in previous centrifuge tests (Xu et al. 2021b), they were well investigated. It was found that the building's length/width primarily influences the differential settlements of the foundation, while its effect on the horizontal displacements of the footings depends on the footing locations.

3.2 Effects of building stiffness

In tunnel-building interaction, building stiffness plays an important role. Figure 6 presents the numerical results of settlements and horizontal displacements of footings and underlying soil for long central frame cases with varying building stiffness at a tunnel volume loss of $V_{l,t}$=2.0%. As expected, an increase in building stiffness reduces the differential settlements (thus deformation) of framed buildings, consistent with the results of surface frames (Xu et al. 2021b). Interestingly, central footings (foot-3, foot-4 and foot-5) and external footings (foot-1, foot-2, foot-6 and foot-7) for the

frames with a higher stiffness settle less and more, respectively, than for the flexible frames. This is closely related to the load redistribution and building shear stiffness (Xu et al. 2025). Similar phenomena can also be observed in the deep tunnel cases (Figure 6(b)), with a smaller influence of building stiffness on the footing settlements for a deeper tunnel scenario.

In the horizontal direction, Figures 6(c) and (d) show that the effect of building stiffness on the horizontal displacements of footings is also notable: the greater the stiffness, the smaller the horizontal displacements for all footings. Notably, although the maximum horizontal displacement of the footings is greater for the shallow tunnel scenarios than for the deep tunnel models, the horizontal displacements of the specific footings may be greater for deep tunnel tests than for the shallow tunnel cases. For instance, foot-2 and foot-6 in deep tunnel modes (Figure 6(d)) show a greater horizontal displacement than those in shallow tunnel cases (Figure 6(c)). This is due to the difference of the distributions of soil horizontal displacements in the two tunnel depths.

The effect of building stiffness on short frame cases (symmetric or eccentric) was investigated by Xu et al. (2021a) and is not covered in this paper. It was found that building stiffness also influences the response of short central frames to tunneling, although its effect on the eccentric cases is minor, as short eccentric frames usually exhibit very low level of deformation.

3.3 Effects of footing width

In practice, the width of footings varies between buildings and may play a role in tunnel-footing interaction. To investigate the effect of footing width on tunneling-induced separated footing displacements, Figure 7 presents the numerical results of the vertical (U_z) and horizontal (U_x) displacements of separated footings and underlying soil for the long central frames with varying footing widths at $V_{l,t}$=2.0%. Results show a minor influence of footing width on the settlement and

horizontal displacements of both the footings and soil within the investigated range of footing width. As expected, the building with wider footings shows a slightly smaller settlement. However, Figure 7(b) also shows smaller horizontal displacements for footings with greater width, which may be attributed to their reduced rotational degrees of freedom.

3.4 Subsurface soil displacement contours

To gain further insights into the soil displacement mechanisms, this section considers contours of soil settlements (Figure 8) and horizontal displacements (Figure 9) for selected tests. Figure 8 shows that, compared against the greenfield settlement presented in Figure 8(a), the presence of the long central frames primarily increases the settlement of the soil around the footings, while the settlement of deeper soil is slightly reduced. Furthermore, a flexible long frame tends to increase the settlement of the soil above the tunnel (compare (c) and (d), or (i) and (j)), while slightly reducing the settlement of the soil around the external footings (foot-1, foot-2, foot-6 and foot-7). As expected, the effect of footing width on soil settlement contours is minor, with the soil settlement zones around footings being narrower and deeper for the frame with a smaller footing width. On the other hand, short eccentric frames may increase the overall settlement level of underlying soil depending on the building pressure. For all scenarios, a heavier building increases the level of the settlement of the soil of the entire zone (compare (e) and (f), or (k) and (l), or (m) and (n)). Finally, it was found that tunnel depth mainly affects the magnitude and the width of the settlement zones.

The effects of separated footings on the horizontal displacements of subsurface soil due to tunneling are now considered. Figure 9 shows that long central frames with separated footings provide significant alteration to the subsurface soil movements in the horizontal direction, with the displacement field of the shallow soil being separated into several zones by the footings. The roles of

building stiffness (compare (c) and (d), or (i) and (j)), foundation pressure (compare (e) and (f)) and footing width (compare (g) and (h)) on tunnel-soil-footing interaction are minor for long central frame cases. However, the foundation pressure plays a role in tunnel-soil-footing interaction for short eccentric frame cases: the greater the pressure, the larger the horizontal displacements of the soil beneath the foundation (compare (k) and (l), or (m) and (n)). Again, tunnel cover depth shows a negligible influence on the horizontal displacement field distribution of the soil due to tunneling.

3.5 Superstructure deformation and level of damage

3.5.1 Horizontal strain and shear distortion

Xu et al. (2021) has experimentally confirmed that the horizontal strains at the foundation level for buildings with separated footings are significant. In this study, the horizontal strain ε_h at each panel is computed by dividing the differential horizontal displacements of neighboring footings by their distance. Figure 10 presents the footing displacements (vertical U_z and horizontal U_x) and horizontal strains (ε_h >0 indicates tension strain) of long central frames against tunnel volume loss $V_{l,t}$, with C/D=1.3. Only the results of Foot-1 to Foot-4 are presented, considering the symmetric response of the long central frames to tunneling. To facilitate the comparison, greenfield results at nominal locations of the footings are also included in Figure 10(a).

First, the effects of building stiffness, foundation pressure and footing width on footing displacements are considered. Figure 10 shows that the settlements and horizontal displacements of all footings/panels increase with tunnel volume loss. Furthermore, results in Figure 10(b) suggest the influence of structure stiffness on footing displacements depends on the magnitude of tunnel volume loss $V_{l,t}$: at a small $V_{l,t}$, building stiffness plays a minor role, while its effect on footing displacements becomes greater for a larger tunnel volume loss ($V_{l,t}$ >1.0%). This is primarily due to the formation

of a gap between the surface and the undersides of the central footings at a higher $V_{l,t}$ for the case with a stiffer building. Figures 10(c) and (d) show that a greater building density or a smaller footing width also results in greater footing displacements. The foundation pressure (density ρ) mainly affects footing settlements, while footing width primarily influences the horizontal displacements of the footings.

The horizontal strain ε_h at the foundation levels are now discussed. For all the long central frames, Figure 10 shows that panel-1 and panel-2 show tension distortion while panel-3 exhibit compressive deformation, consistent with the greenfield results. Furthermore, horizontal strains for all panels show an increasing trend with tunnel volume loss ($V_{l,t}$), and the absolute values of compressive strains are always greater than those of tensile strains. This suggests that the compressive deformation should be particularly noted in tunneling projects. Notably, the influences of building stiffness (Young's modulus E), foundation pressure (density ρ) and footing widths on panel horizontal strains are minor, and the variation of horizontal strain ε_h with the above parameters is qualitatively the same as that of footing displacements. Finally, it is found that footing displacements and panel horizontal strains are comparable with the greenfield data, suggesting the potential use of greenfield results as a conservative estimation of the distortion of buildings with separated, embedded footings when subjected to tunneling-induced displacements.

The roles of tunnel cover depth and building geometry on tunnel-footing interaction are discussed using the data presented in Figure 11. Results in Figure 11(b) indicate the same role of building stiffness (Young's modulus E) in footing displacements and panel horizontal distortion in the deeper tunnel scenarios (C/D=2.0) as in the shallower tunnel models (C/D=1.3, Figure 10(b)). Interestingly, footing displacements are greater for short eccentric frames than for long central frames,

while the horizontal strains for both frames are nearly identical (compare (b) and (c)). As expected, shallower tunnels usually lead to greater displacements and horizontal strains (compare Figures 11(c) and (d), or Figures 10(b) and 11(b)).

To gain further insights into the effects of building stiffness and foundation pressure on panel horizontal strain and shear distortion, Figure 12 presents the variation of maximum horizontal strains ε_h and building shear distortion β_{max} with Young's modulus E and building material density ρ at $V_{l,t}$ =2.0%. In this study, the shear distortion parameter β proposed by Son and Cording (2005) was used and was calculated using the top and bottom corner displacements of each panel by subtracting tilt from the slope. The shear distortion parameter was chosen because the centrifuge results obtained by Xu et al. (2020) show that the framed buildings primarily exhibit shear distortion.

As expected, results in Figures 12(a) and (b) suggest a decreasing trend of building maximum shear distortion and horizontal strains with stiffness (Young's modulus E), with a greater influence of building stiffness on the shear distortion than on the horizontal strain. Furthermore, Figures 12(c) and (d) show that the influences of foundation pressure on building distortion and panel horizontal strains tend to be secondary within the investigated range, with a slight increasing trend with the building material density. This is primarily due to the fact that the two-story building with separated footings is relatively "flexible" in tunnel-building interaction, resulting in a small or negligible gap between the soil and the undersides of the footings. Therefore, a further increase in foundation pressure would not significantly increase the building distortion. Finally, Figure 12(c) shows that short eccentric buildings exhibit smaller distortion than long central frames (consistent with Xu et al. 2021b), while the horizontal strains for the short frames may be greater than for the long frames. This finding is crucial for practical engineering projects and should be given careful consideration.

3.5.2 Building damage level

To visually illustrate the building distortion, Figure 13 presents frame deformed shapes in selected models, along with the maximum tensile strain within panels. Furthermore, the level of building is also linked with the thresholds of limiting tensile strain defined by Son and Cording (2005) summarized in Table 3. In Figure 13, the level of damage is denoted by a color scheme.

To compute the maximum tensile strain ε_{max} within panels, Mohr's circle of strain is used, and $\varepsilon_{max} = \frac{\varepsilon_h}{2} + \sqrt{\frac{1}{4}\varepsilon_h^2 + \varepsilon_d^2}$ can be obtained under the plane strain condition scenario, where ε_d denotes the diagonal strain. For the second story panels, the horizontal strains ε_h are negligible due to the high axial stiffness of the continuous beams. Therefore, the values of ε_h of the second story panels can be directly computed using $\varepsilon_{max} = \varepsilon_d$. Xu et al. (2020) suggested the diagonal strain can be directly computed using $\varepsilon_d = \beta/2$ for shear-dominated buildings (bending distortion is negligible). Using the above equation, the values of ε_{max} for all panels were computed and linked to the category of damage. Figure 13 presents the results of selected frames, along with the deformed frame shapes, at $V_{l,t}$=2.0%.

Results in Figure 13 confirm that an increase in building stiffness reduces the panel distortion (compare (a) and (b), or (g) and (h)), and a heavier building shows greater tensile strains within panels (compare (c) and (d), or (i) and (j)). Furthermore, the effect of footing width on panel distortion is negligible, while a deeper tunnel tends to reduce the level of damage of the building. The conclusion that the short eccentric frame exhibits smaller distortion than the long central building is numerically verified (Xu et al. 2021). It is also found that the levels of damage for all panels are not greater than category 2, with panel-2 and panel-5 of long central frames and the lower panel-1 of short eccentric frames showing the greatest distortion. Finally, the values of ε_{max} for the first story panels differ from those for the second story panels due to the large horizontal strains between footings.

3.6 Relative stiffness and modification factor

In engineering projects, the method of modification factor may be adopted to quickly evaluate tunneling-induced damage. Xu et al. (2020) proposed shear distortion modification factor M^{β}, defined as: $M^{\beta}=\frac{\beta_{max}}{\overline{GS}_{max}}$ to predict the shear deformation of a building subjected to tunneling-induced movements, where $\overline{GS}_{max}$ denotes the maximum greenfield slope, defined as the maximum slope of a movable line segment with a length equal to a bay width on the greenfield settlement curve. Then, M^{β} is correlated to the relative soil-building shear stiffness κ, computed by $\kappa=\frac{E_s B}{GA_s^*}$, where E_s and GA_s^* are the representative soil stiffness and the plane strain building shear stiffness, respectively. In this paper, the value of E_s was calculated using the approach proposed by Farrell (2010), based on the average soil shear strains at the mid-depth of the tunnel crown in the FE models and triaxial test results from Zhao (2008). GA_s^* was obtained using three-point or four-point loading tests conducted on numerical models (Xu et al. 2025).

Similarly, Goh and Mair (2014) defined an analogous modification factor $M^{\varepsilon,h}$ for the horizontal strain of the building. The value of $M^{\varepsilon,h}$ can be computed by dividing the maximum horizontal strains ε_{max} among all bays by the maximum greenfield horizontal strains $\varepsilon_{max,gf}$. Finally, $M^{\varepsilon,h}$ is linked to the relative soil-footing stiffness $\alpha_f^*=\frac{1}{E_s h_f^2}\frac{3K_bK_c}{(2K_b+3K_c)}$, which was modified by Franza et al. (2017), where $K_b=(EI/w_p)_b$ and $K_c=(EI/h_f)_c$ are the average line stiffness of the beam and footing column, respectively; EI is the bending stiffness of the beam/column; w_p is the panel width; h_f is the height of the footing column.

Using the numerical data at a tunnel volume loss of $V_{l,t}$ =2.0% and the above equations, the values of modification factors and relative stiffness are computed. Figure 14 shows the shear distortion modification factor M^{β} against relative soil-building stiffness κ. Upper and lower envelopes

derived by Xu et al. (2021b) using the centrifuge results of surface frames with separated footings are also presented in Figure 14. Results show that the numerical results considering the influences of building stiffness and foundation pressure are in good agreement with the empirical envelopes for both the central and eccentric scenarios. The variation of shear distortion modification factors with building stiffness (Young's modulus E) and foundation pressure (building material density ρ) is also clearly captured by the envelopes. These results suggest that the empirical envelopes derived based on the response of framed buildings on surface footings to tunnel construction are also applicable for the prediction of deformation of buildings with embedded footings.

Finally, the modification factors of horizontal strain $M^{\varepsilon,h}$ are also presented in Figure 15, against the relative soil-footing stiffness α_f^* at $V_{l,t}$ =2.0%. Again, the upper and lower envelopes derived by Franza et al. (2017) for the prediction of tunneling-induced piled structure deformation are also included in Figure 15. Results show that most of the data points (except for the short eccentric frame with C/D=1.3 tunnel models in tensile deformation mode) of $M^{\varepsilon,h}$ are within the empirical envelopes, suggesting the effectiveness of the envelopes in predicting the horizontal distortion of buildings on separated footings. Furthermore, the dependency of horizontal strain modification factor with building stiffness and foundation pressure is also reflected by the results in Figure 15 through relative soil-footing stiffness. Finally, Figure 15(a) shows that short frames (models No. 18-25) usually display larger tensile strain modification factors than the long frames, while results in Figure 15(b) suggest that the values of compressive strain modification factors for all models are similar.

4 Conclusions

A comprehensive numerical study into the effects of foundation pressure and building stiffness on tunneling-induced deformation to framed buildings with separated footings has been presented, with

the aim to provide insights into the building damage assessment for urban tunneling projects. The paper considered two-story framed buildings with separated footings, embedded 1.0 m into ground, and subjected to tunneling-induced displacements in sand. A hypoplastic soil constitutive model was adopted to simulate the sand behavior and soil-structure interaction mechanism, with the detailed parameters calibrated using element tests and centrifuge data.

Results highlight the important roles of building stiffness and foundation pressure on the settlements and horizontal displacements of footings due to tunneling, particularly for a larger tunnel volume loss $V_{l,t}$. Importantly, an increase in building stiffness reduces both the vertical and horizontal displacements of footings, while a greater foundation pressure primarily increases the settlements of the footings. On the other hand, footing width only plays a role in determining the horizontal displacements of the footings, with a greater footing width exhibiting smaller horizontal displacements. Short eccentric frames usually display greater footing displacements in both vertical and horizontal directions.

The presence of framed buildings on separated footings also significantly alters the subsurface soil movements. Long central frames primarily increase the settlement of the soil around the footings, while short eccentric frames may increase the overall settlement level of underlying soil depending on the building pressure. For all frames, a heavier building increases the settlement level of the soil in the entire zone. A flexible long frame tends to increase the settlement of the soil above the tunnel, while slightly reducing the settlement of the soil around the external footings. Separated footings provide significant alteration to the subsurface soil movements in the horizontal direction, with the displacement field of the shallow soil being separated into several zones by the footings. The roles of building stiffness, foundation pressure and footing width on tunnel-soil-footing interaction are minor

for long central frame cases. Only the foundation pressure plays a role in tunneling-induced movements for short eccentric frame cases.

Deformation parameters including shear distortion and horizontal strain are used to quantify the distortion of framed buildings to tunnel construction. For all considered buildings, external panels (panel-1 and panel-2) show tension distortion while central panels (panel-3) exhibit compressive deformation. The influences of building stiffness and foundation pressure on panels horizontal strains are minor for the investigated parameter ranges, while their influences on building shear distortion are significant. Footing displacements and panel horizontal strains are comparable with the greenfield data, suggesting the potential use of greenfield results as a conservative estimation of the distortion of buildings with separated, embedded footings when subjected to tunneling-induced displacements. Modification factors of shear distortion and horizontal strains are presented, and are in good agreement with the empirical envelopes, demonstrating the effectiveness of existing approaches.

The above conclusions highlight the need to consider building stiffness and foundation pressure in the evaluation of tunneling-induced building deformation in both horizontal and vertical directions. Future study could consider the influences of soil density and type, column stiffness, infilling wall and tunnel excavation process on the tunnel-building interaction topic.

Acknowledgments

This research has received funding from the National Natural Science Foundation of China (Grant No. 52108364, 52478389) and the Royal Society, UK (Grant No. 211179).

Data Availability Statement

Data generated or analyzed during this study are available from the corresponding author upon reasonable request.

Author contributions

Data curation: YW, MG

Formal analysis: YW, MG, JX

Funding acquisition: JX

Investigation: JX

Methodology: JX, MG, JN, LC

Supervision: JX, JN, LC

Writing – original draft: JX

Writing – review & editing: JX, JN, LC

Competing interests

The authors declare there are no competing interests.

References

Boldini, D., Losacco, N., Bertolin, S., Amorosi, A., 2018. Finite element modelling of tunneling-induced displacements on framed structures. Tunneling and Underground Space Technology, 80 (April), 222–231.

Boldini, D., Losacco, N., Franza, A., DeJong, M., Xu, J., Marshall, A., 2021. Tunneling induced deformation of bare frame structures on sand: numerical study of building deformations. J. Geotech. Geoenviron. Eng. 147 (11), 04021116.

Boonsiri, I. & Takemura, J. (2015). Observation of ground movement with existing pile groups due to tunneling in sand using centrifuge modelling. Geotechnical and Geological Engineering, 33, No. 1, 621–640.

Burland, J. B., Broms, B. B., and De Mello, V. F. B. (1977). Behaviour of foundations and structures. In Proceedings of the 9th International Conference on Soil Mechanics and Foundations Engineering, volume 2, pages 495–546, Tokyo.

Cheng, C.Y., Dasari, G.R., Chow, Y.K. and Leung, C.F., 2007. Finite element analysis of tunnel–soil–pile interaction using displacement controlled model. Tunneling and Underground Space Technology, 22(4), pp.450-466.

Elkayam, I. and Klar, A. (2019). Nonlinear elasto-plastic formulation for tunneling effects on superstructures. Canadian Geotechnical Journal, 56(7):956–969.

Farrell, R.P. Tunnelling in sands and the response of buildings. PhD thesis, 2011, University of

Cambridge.

Franza, A., Acikgoz, S. and DeJong, M.J., 2020. Timoshenko beam models for the coupled analysis of building response to tunneling. Tunneling and Underground Space Technology, 96, p.103160.

Franza, A., DeJong, M.J., 2019. Elastoplastic solutions to predict tunneling-induced load redistribution and deformation of surface structures. Journal of Geotechnical and Geoenvironmental Engineering, 145 (4), 04019007.

Franza, A., Marshall, A.M., Haji, T., Abdelatif, A.O., Carbonari, S. and Morici, M., 2017. A simplified elastic analysis of tunnel-piled structure interaction. Tunneling and Underground Space Technology, 61, pp.104-121.

Franza, A., Miraei, S., Boldini, D. and Losacco, N., 2022. An equivalent beam approach for assessing tunnelling-induced distortions of frames with infills. Tunnelling and Underground Space Technology, 129, p.104686.

Franzius, J.N., Potts, D.M., Addenbrooke, T.I. and Burland, J.B., 2004. The influence of building weight on tunnelling-induced ground and building deformation. Soils and foundations, 44(1), pp.25-38.

Giardina, G., DeJong, M.J. and Mair, R.J., 2015. Interaction between surface structures and tunnelling in sand: Centrifuge and computational modelling. Tunnelling and Underground Space Technology, 50, pp. 465-478.

Goh, K.H., Mair, R.J., 2014. Response of framed buildings to excavation-induced movements. Soils and foundations, 54 (3), 250–268.

Herle, I., Gudehus, G., 1999. Determination of parameters of a hypoplastic constitutive model from properties of grain assemblies. Mechanics of Cohesive-frictional Materials, 4 (5), 461–486.

Hibbitt, K., 2002. ABAQUS/Explicit User's Manual: Version 6.3. Hibbit, Karlsonn & Sorensen.

Khalajzadeh, A.K., Choobbasti, A.J. and Kutenaei, S.S., 2023. Dynamic behaviour of a circular tunnel in the sand: A numerical verification of a centrifuge program. Tunneling and Underground Space Technology, 138, p.105152.

Lanzano, G., Visone, C., Bilotta, E. and Santucci de Magistris, F., 2016. Experimental assessment of the stress–strain behaviour of Leighton Buzzard sand for the calibration of a constitutive model. Geotechnical and Geological Engineering, 34, pp.991-1012.

Mair, R.J., Taylor, R.N., Burland, J.B., 1996. Prediction of ground movements and assessment of risk of building damage due to bored tunneling. In: Mair, R.J., Taylor, R.N. (Eds.), Proceedings of the International Symposium on Geotechnical Aspects of Underground Construction in Soft Ground. Balkema, Rotterdam, London, United Kingdom, pp. 713–718.

Mair, R.J. and Taylor, R.N., 1999. Bored tunnelling in the urban environments. In: Publication committee (Eds.), Proceedings of the 14th International Conference on Soil Mechanics and Foundation Engineering. Hamburg, Germany, pp. 2353–2385.

Maleki, M., Sereshteh, H., Mousivand, M. and Bayat, M., 2011. An equivalent beam model for the analysis of tunnel-building interaction. Tunneling and Underground Space Technology, 26(4),

pp.524-533.

Miliziano, S., Caponi, S., Carlaccini, D. and de Lillis, A., 2022. Prediction of tunneling-induced effects on a historic building in Rome. Tunneling and Underground Space Technology, 119, p.104212.

Ng, C.W.W., Hong, Y., Liu, G.B. and Liu, T., 2012. Ground deformations and soil–structure interaction of a multi-propped excavation in Shanghai soft clays. Géotechnique, 62(10), pp.907-921.

Ng, C. W., Wong, Y. Y. A., and Shakeel, M. (2022). Effects of the skew angle of new tunneling on an existing tunnel: three-dimensional centrifuge and numerical modeling. Canadian Geotechnical Journal, 233 59(10), 1728–1742.

Pickhaver, J.A., Burd, H.J. and Houlsby, G.T., 2010. An equivalent beam method to model masonry buildings in 3D finite element analysis. Computers & structures, 88(19-20), pp.1049-1063.

Potts, D.M., Addenbrooke, T.I., 1997. A structure's influence on tunneling-induced ground movements. Proceedings of the Institution of Civil Engineers-Geotechnical Engineering, 125 (2), 109–125.

Ritter, S., Giardina, G., DeJong, M.J. and Mair, R.J., 2018. Centrifuge modelling of building response to tunnel excavation. International Journal of Physical Modelling in Geotechnics, 18(3), pp.146-161.

Shi, J., Chen, Y., Lu, H., Ma, S., and Ng, C. (2022). Centrifuge modeling of the influence of joint stiffness on pipeline response to underneath tunnel excavation. Canadian Geotechnical Journal, 59(9), 1568–1586.

Son, M. and Cording, E. J. (2005). Estimation of Building Damage Due to Excavation-Induced Ground Movements. Journal of Geotechnical and Geoenvironmental Engineering, 131(2):162–177.

Song, G., Marshall, A.M., 2020. Centrifuge modelling of tunneling induced ground displacements: pressure and displacement control tunnels. Tunneling and Underground Space Technology, 103, p.103461.

Song, G., Xu, J., & Marshall, A. M. (2023). Numerical study on the effect of protective wall depth in reducing structure deformations caused by tunneling. Computers and Geotechnics, 158, Article 105374.

Von Wolffersdorff, P.-A., 1996. A hypoplastic relation for granular materials with a predefined limit state surface. Mechanics of Cohesive-frictional Materials, 1(3), 251–271.

Xu, J., Franza, A. & Marshall, A. M. (2020). Response of framed buildings on raft foundations to tunneling. Journal of Geotechnical and Geoenvironmental Engineering, 146, No. 11, 04020120.

Xu, J., Franza, A., Marshall, A.M., Losacco, N., 2021a. Role of footing embedment on tunnel–foundation interaction. Journal of Geotechnical and Geoenvironmental Engineering, 147 (9), 06021009.

Xu, J., Franza, A., Marshall, A.M., Losacco, N., Boldini, D., 2021b. Tunnel–framed building

interaction: Comparison between raft and separate footing foundations. Géotechnique 71 (7), 631–644.

Xu, J., Gui, J. and Sheil, B., 2024. A numerical investigation of the role of basements on tunnel-frame interaction in sandy soil. Computers and Geotechnics, 169, p.106197.

Xu, J., Yu, Z., Chen, R., Xu, T., Chen, C. and Wang, Z., 2025. Evaluation of the shear stiffness and load redistribution of framed structures affected by tunnelling. Computers and Geotechnics, 177, p.106899.

Yu, J., Leung, C., Huang, M., Tan, J.Q.W., 2022. Assessment of settlement-based strain in masonry building facade due to tunneling. Computers and Geotechnics, 144, 104658.

Yu, Y., Franza, A., Ghiassi, B., Neves, L.C. and Marshall, A.M., 2025. Tunnelling-induced wall damage: An appraisal of elastoplastic constitutive models for masonry. Tunnelling and Underground Space Technology, 156, p.106240.

Zhao Y. In situ soil testing for foundation performance prediction. PhD thesis, University of Cambridge, 2008.

List of Figures

envelopes from Franza et al. (2017): (a) tensile strain; (b) compressive strain

Figure S1. Numerical results of footing displacements and soil movements with different model widths (7.1 *D* and 10.0 *D*): (a) and (b) short frame, (c) and (d) long frame

List of Tables

Table 1. Overview of numerical parametric study

No	*C/D*	*B* (m)	*e/B*	*E* (GPa)	ρ (kg/m^3)	b_f (m)	Note
1	1.3	-	-	-	-	-	Greenfield test
2	2.0	-	-	-	-	-	
3	1.3	31.3	0	70	2700	0.82	Building stiffness
4	1.3	31.3	0	50	2700	0.82	
5	1.3	31.3	0	30	2700	0.82	
6	1.3	31.3	0	50	1600	0.82	Foundation pressure
7	1.3	31.3	0	50	3800	0.82	
8	1.3	31.3	0	50	4900	0.82	
9	1.3	31.3	0	50	2700	0.68	Footing width (affecting pressure)
10	1.3	31.3	0	50	2700	0.95	
11	1.3	31.3	0	50	2700	1.09	
12	2.0	31.3	0	70	2700	0.82	Building stiffness Deep tunnel
13	2.0	31.3	0	50	2700	0.82	
14	2.0	31.3	0	30	2700	0.82	
15	2.0	31.3	0	50	1600	0.82	Foundation pressure Deep tunnel
16	2.0	31.3	0	50	3800	0.82	
17	2.0	31.3	0	50	4900	0.82	
18	1.3	15.8	0.5	50	1600	0.82	Foundation pressure Short frame
19	1.3	15.8	0.5	50	2700	0.82	
20	1.3	15.8	0.5	50	3800	0.82	
21	1.3	15.8	0.5	50	4900	0.82	
22	2.0	15.8	0.5	50	1600	0.82	Foundation pressure Short frame Deep tunnel
23	2.0	15.8	0.5	50	2700	0.82	
24	2.0	15.8	0.5	50	3800	0.82	
25	2.0	15.8	0.5	50	4900	0.82	

Table 2. Hypoplastic model parameters

Parameter	φ'_c (°)	h_s (MPa)	n	e_{d0}	e_{i0}	e_{c0}	α	γ
Value	32	1969	0.447	0.624	1.16	1.392	0.08	1.5

Table 3. Level of damage and corresponding tensile strain (Son and Cording, 2005)

Category of damage	Level of damage	Limiting tensile strain (%)
0	Negligible	0-0.05
1	Very slight	0.05-0.075
2	Slight	0.075-0.167
3 to 4	Moderate to severe	0.167-0.333
4 to 5	Severe to very severe	>0.333

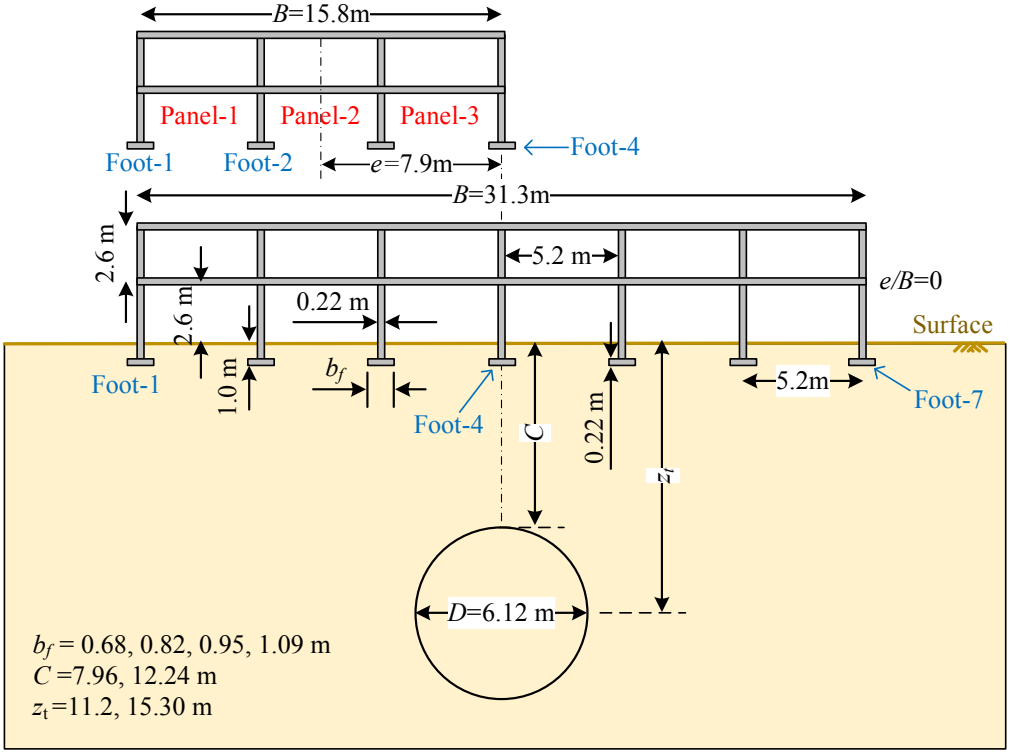

Figure 1. Problem illustration and the definition of model geometric parameters

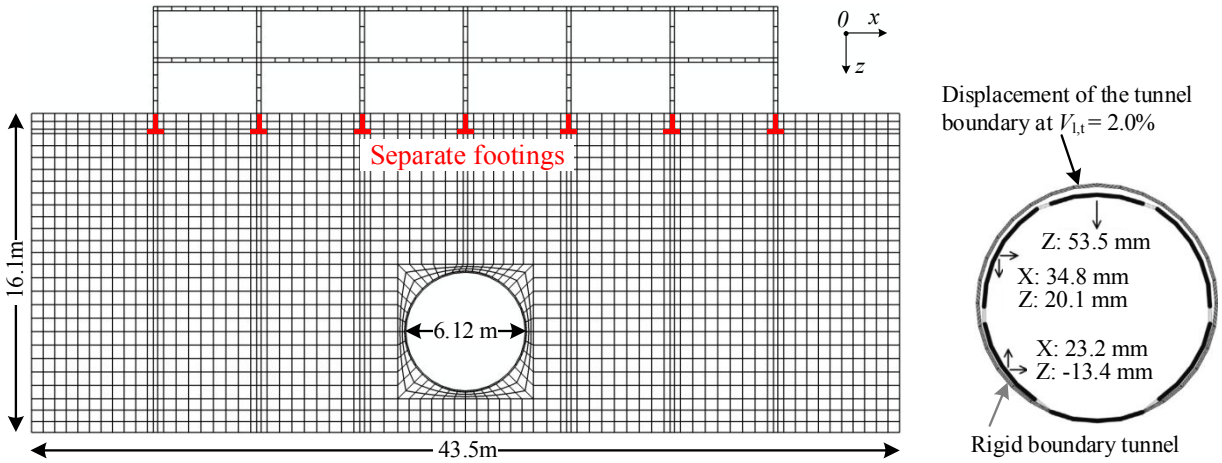

Figure 2. Finite element mesh of test No.3 in Table 1 and imposed displacement boundary conditions

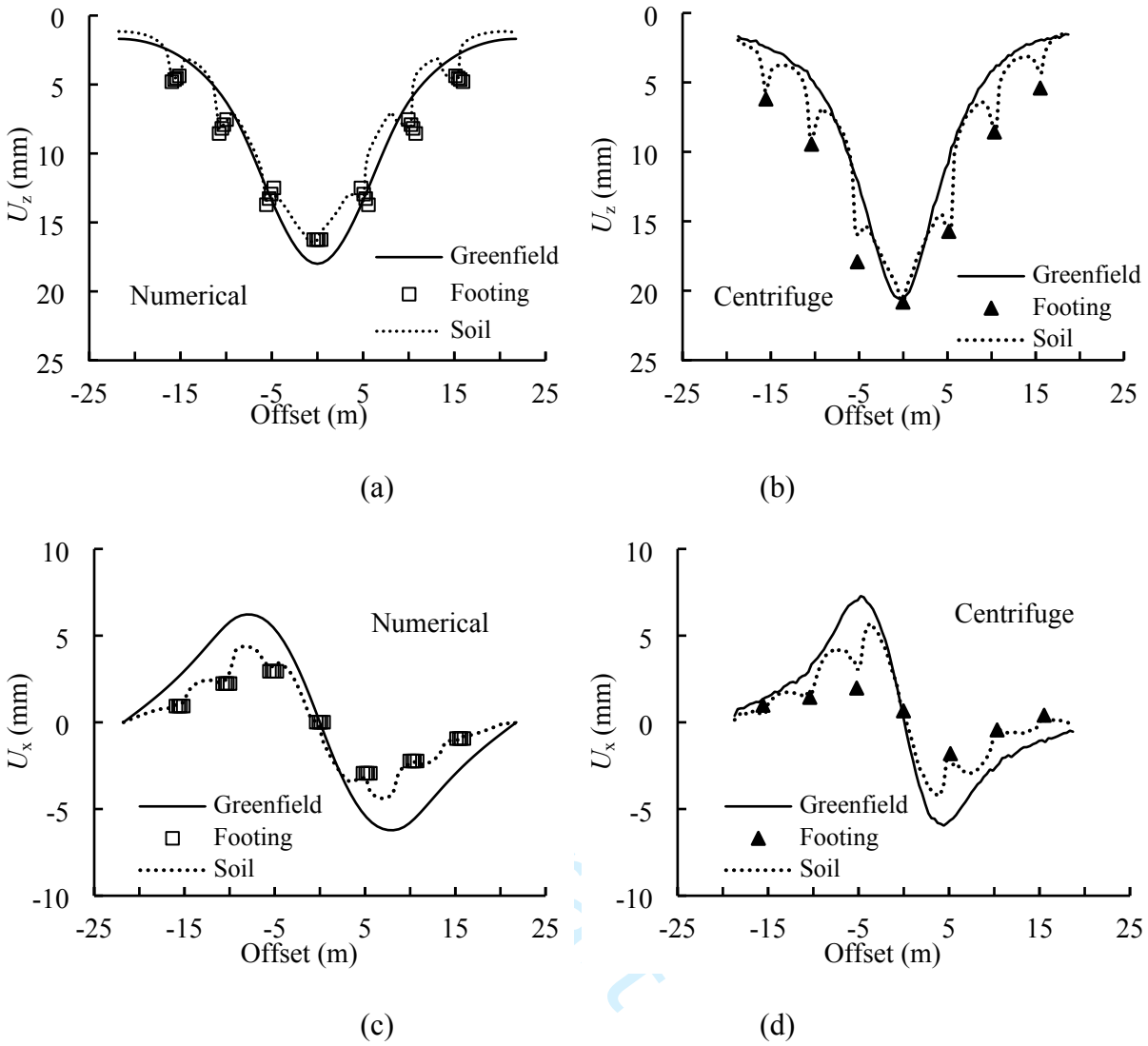

Figure 3. Comparison between FE model predictions (a, c), and centrifuge test measurements (b, d) of surface soil and separated footing displacements at $V_{l,t}$=1.0%; centrifuge data from Xu et al. (2021b)

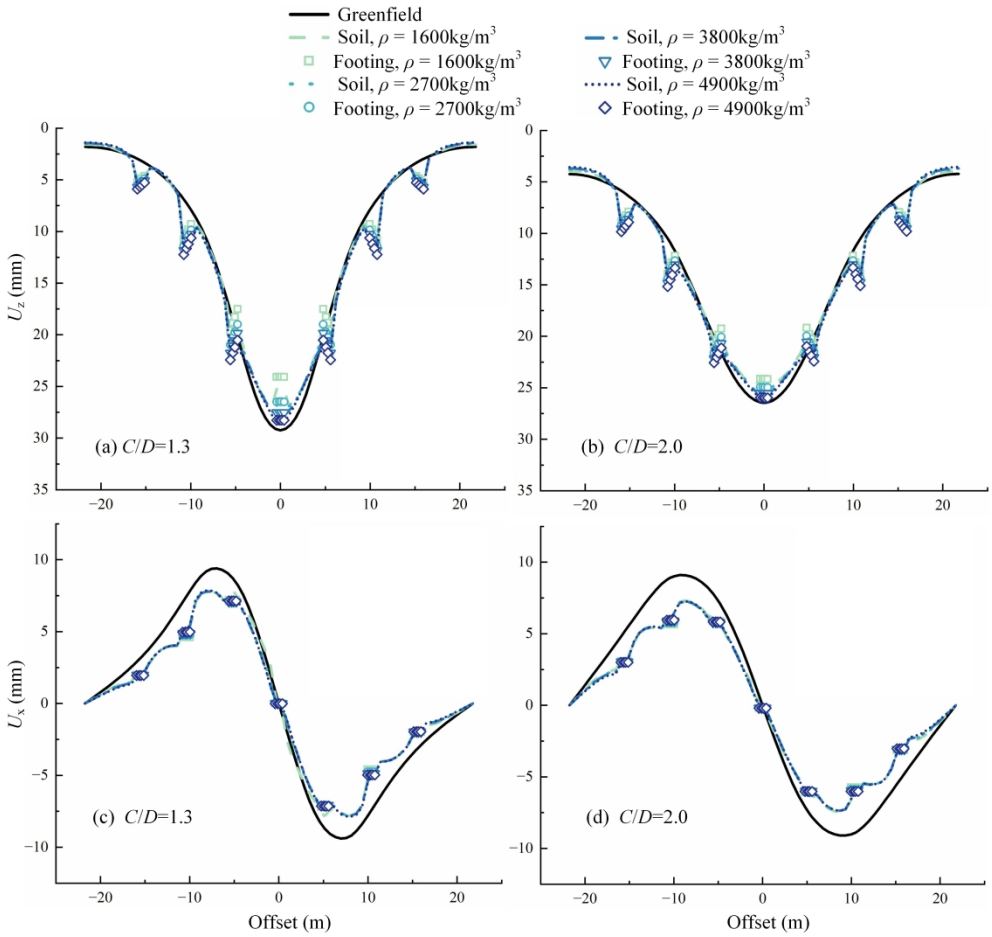

Figure 4. Numerical simulation results of settlements (a, b) and horizontal displacements (c, d) of footings and underlying soil for long central frame cases with varying building material densities: (a, c) *C/D*=1.3, (b, d) *C/D*=2.0

178x168mm (600 x 600 DPI)

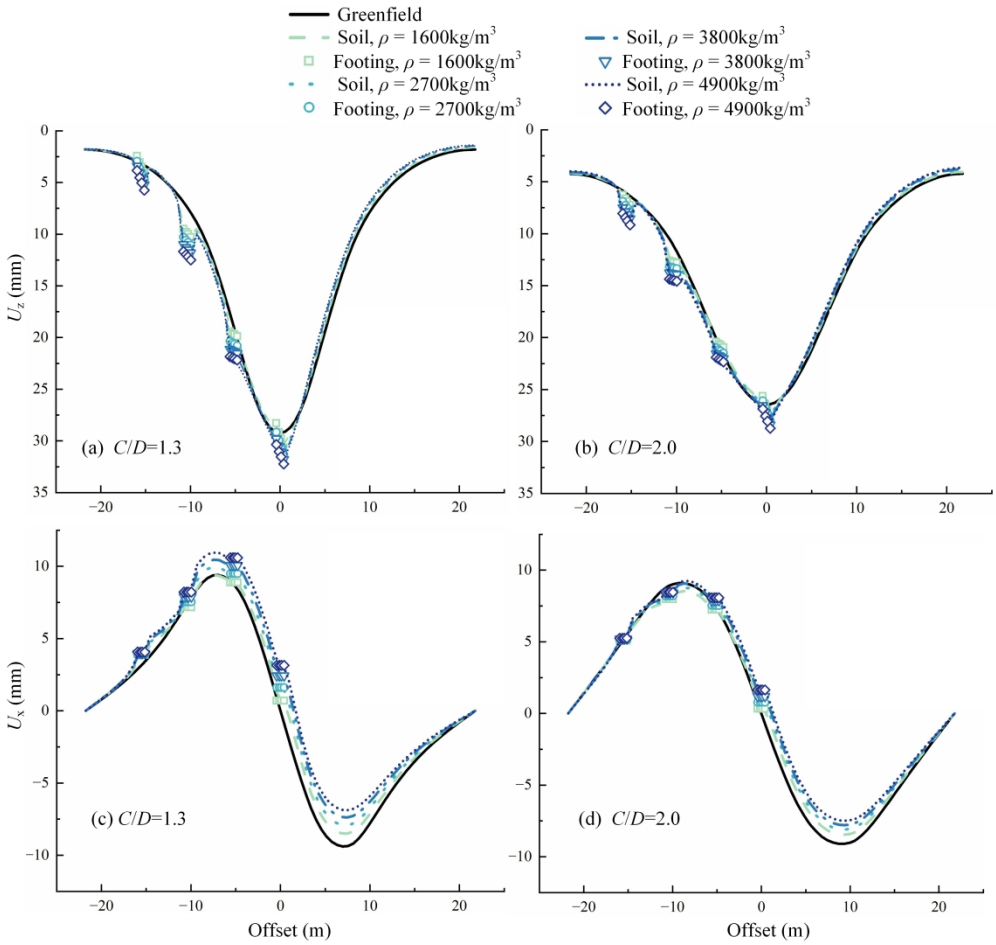

Figure 5. Numerical simulation results of settlements (a, b) and horizontal displacements (c, d) of footings and underlying soil for short eccentric frame cases with varying building material densities: (a, c) *C/D*=1.3, (b, d) *C/D*=2.0

178x169mm (600 x 600 DPI)

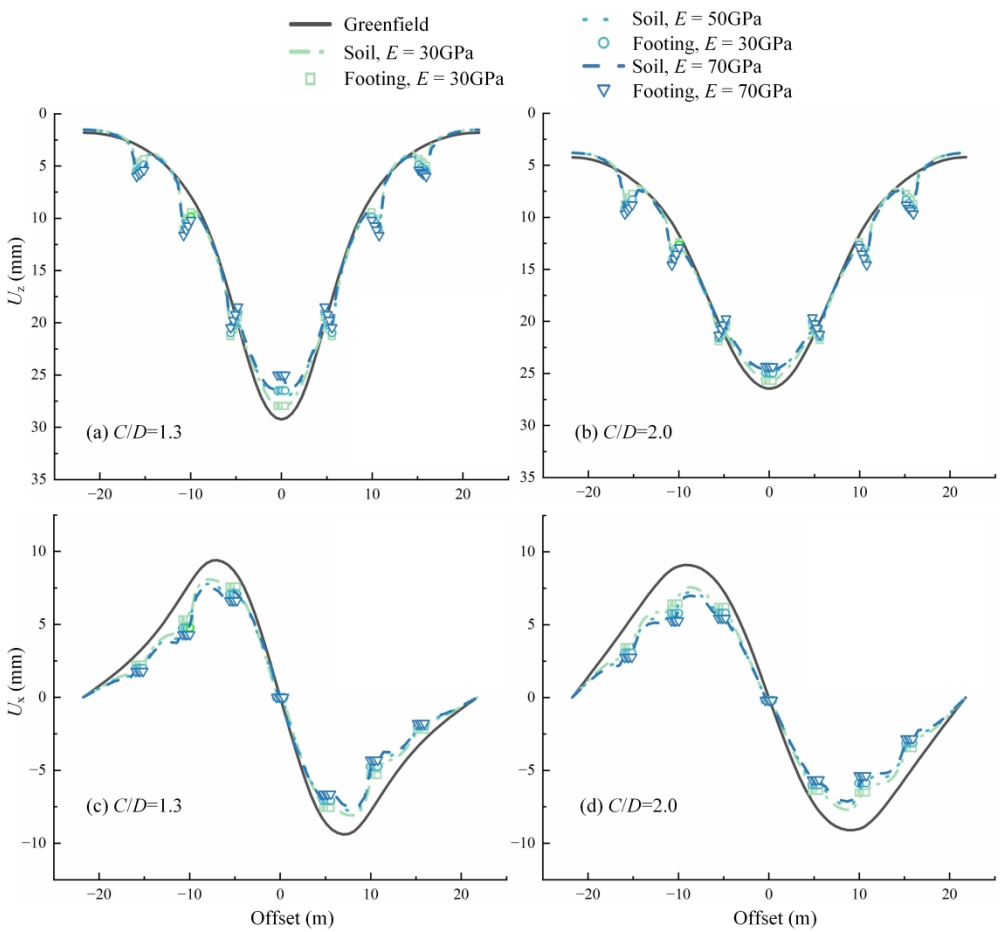

Figure 6. Numerical simulation results of settlements (a, b) and horizontal displacements (c, d) of footings and underlying soil for long central frame cases with varying building stiffness: (a, c) *C/D*=1.3, (b, d) *C/D*=2.0

176x165mm (600 x 600 DPI)

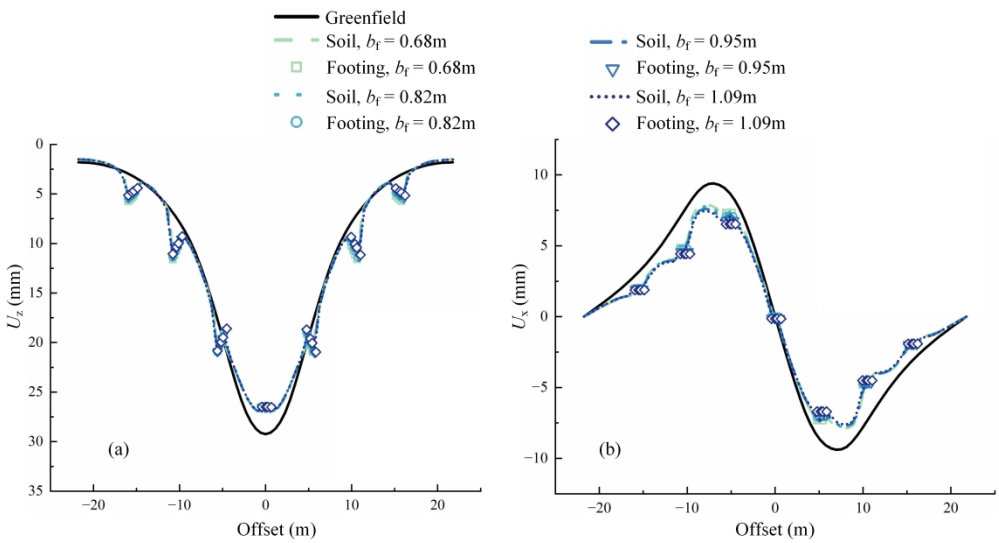

Figure 7. Numerical simulation results of settlements (a) and horizontal displacements (b) of footings and underlying soil for long central frame cases with varying footing widths: *C/D*=1.3

186x101mm (600 x 600 DPI)

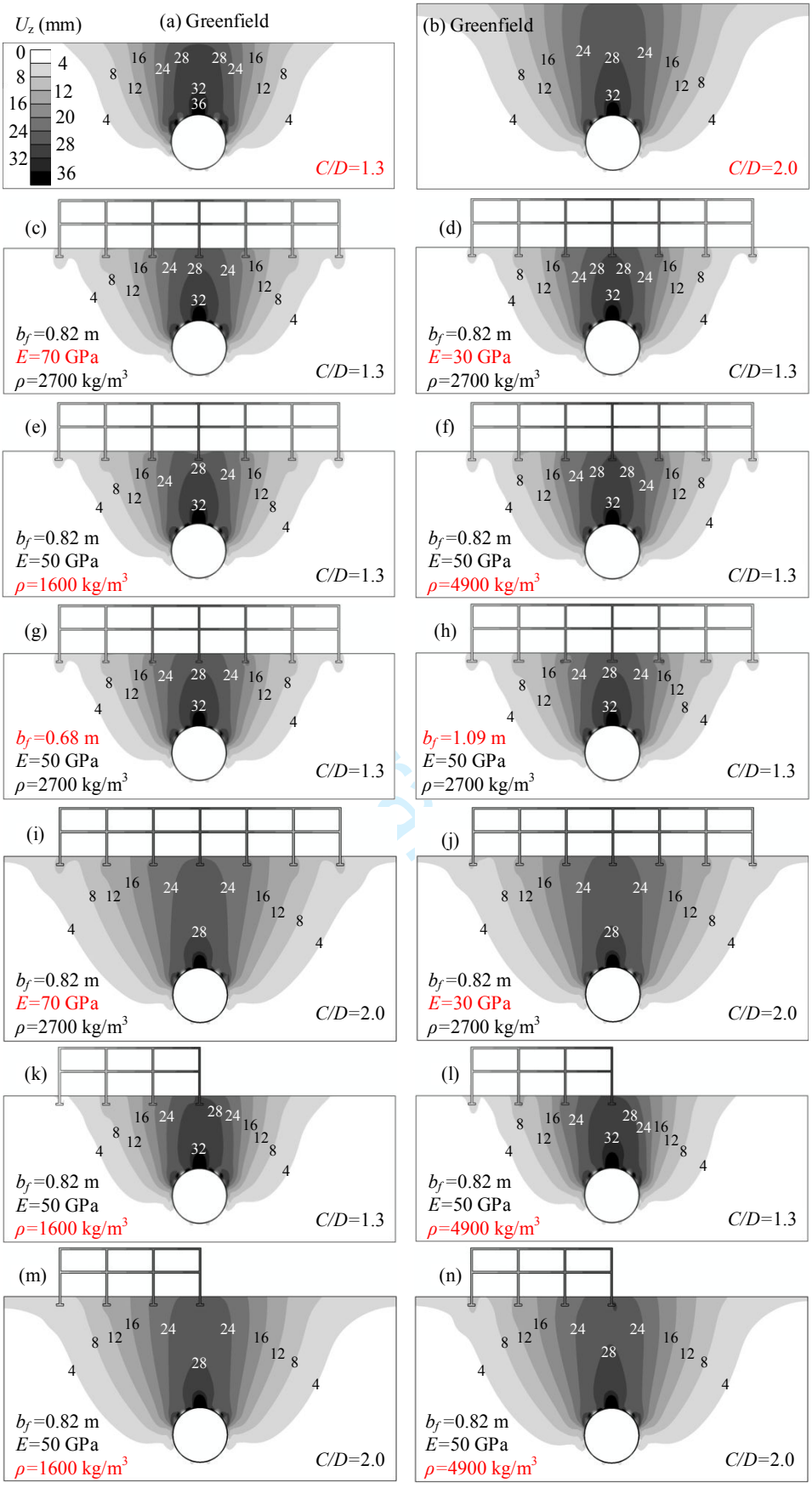

Figure 8. Numerical simulation results of contours of soil settlements U_z in selected tests: greenfield tunneling (a, b) and the effects of building stiffness (c, d), (i, j), foundation pressure (e, f), (k, l), (m, n) and footing size (g, h) on ground movements

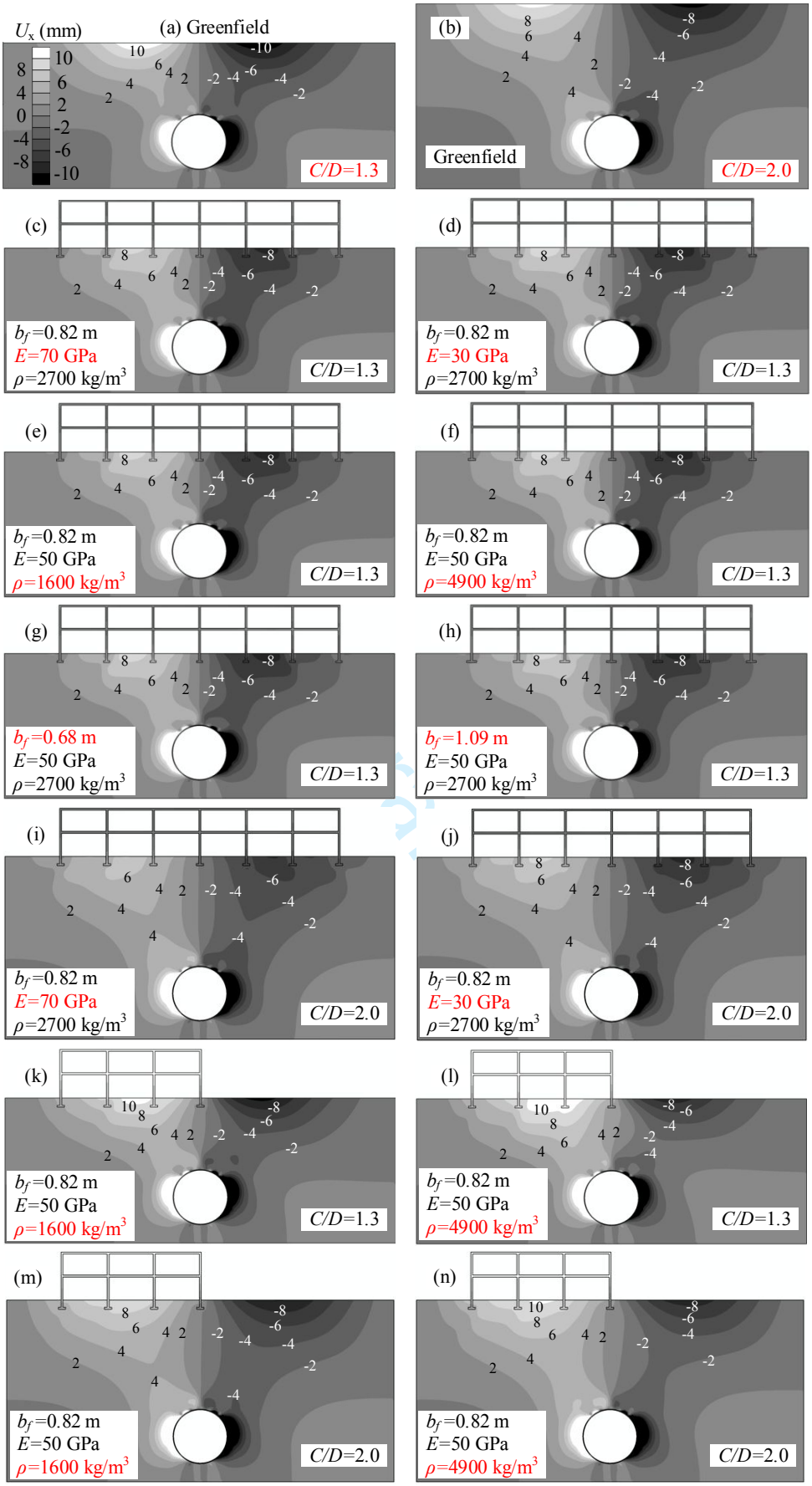

Figure 9. Numerical simulation results of contours of soil horizontal displacements U_x in selected tests: greenfield tunneling (a, b) and the effects of building stiffness (c, d), (i, j), foundation pressure (e, f), (k, l), (m, n) and footing size (g, h) on ground movements

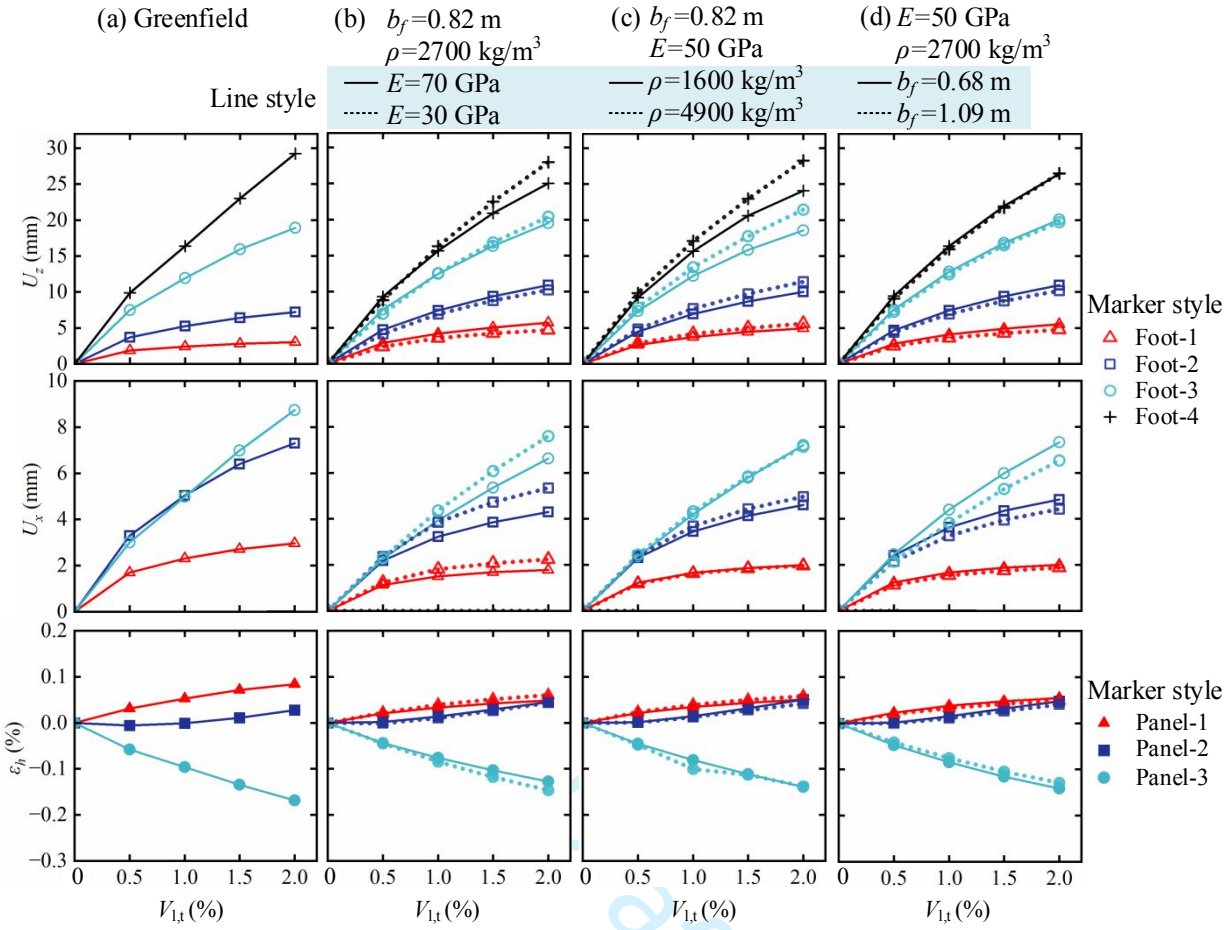

Figure 10. Footing displacements and horizontal strains (ε_h >0 indicates tension strain) of long central frames against $V_{l,t}$, C/D=1.3: (a) greenfield displacements and strains at the nominal locations of the footings, and the influences of (b) building stiffness, (c) foundation pressure and (d) footing width

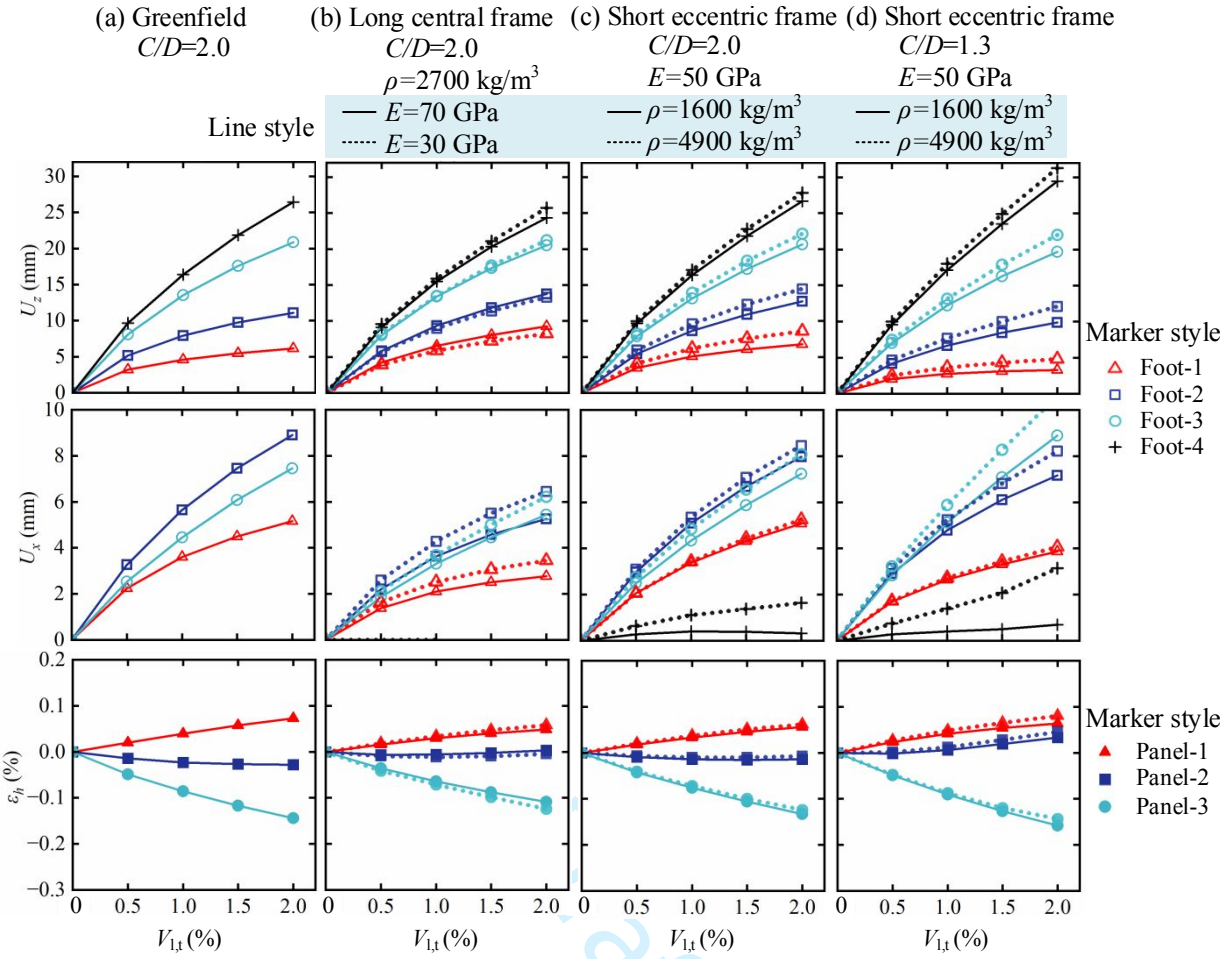

Figure 11. Footing displacements and horizontal strains (ε_h >0 indicates tension strain) against $V_{l,t}$, b_f=0.82 m: (a) greenfield displacements and strains at the nominal locations of the footings, and the influences of (b) building stiffness and (c, d) foundation pressure

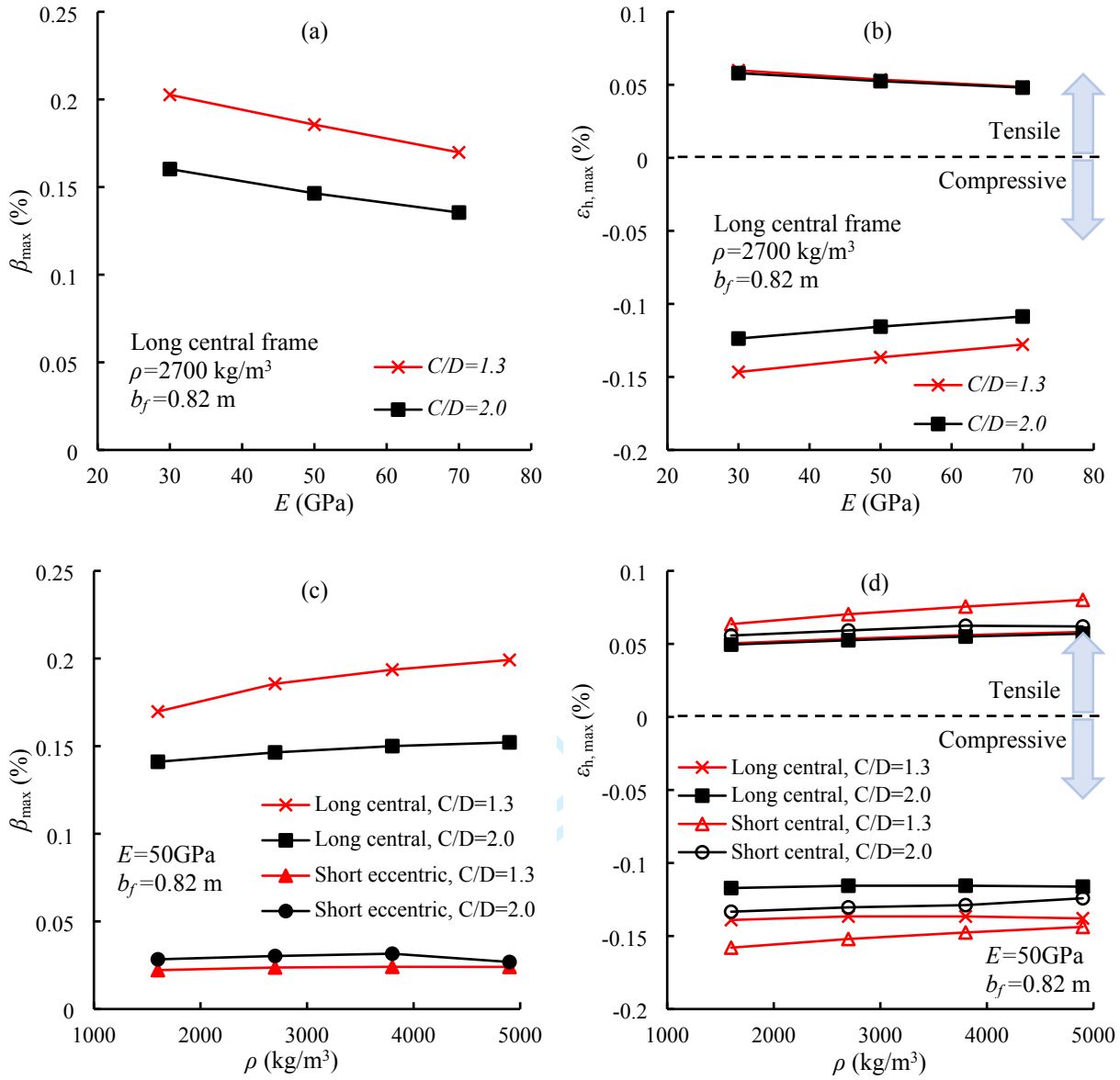

Figure 12. Variation of (a, c) maximum building shear distortion β_{max} and (b, d) horizontal strains ε_h (ε_h >0 indicates tension strain) with (a, b) Young's modulus E, and (c, d) density ρ

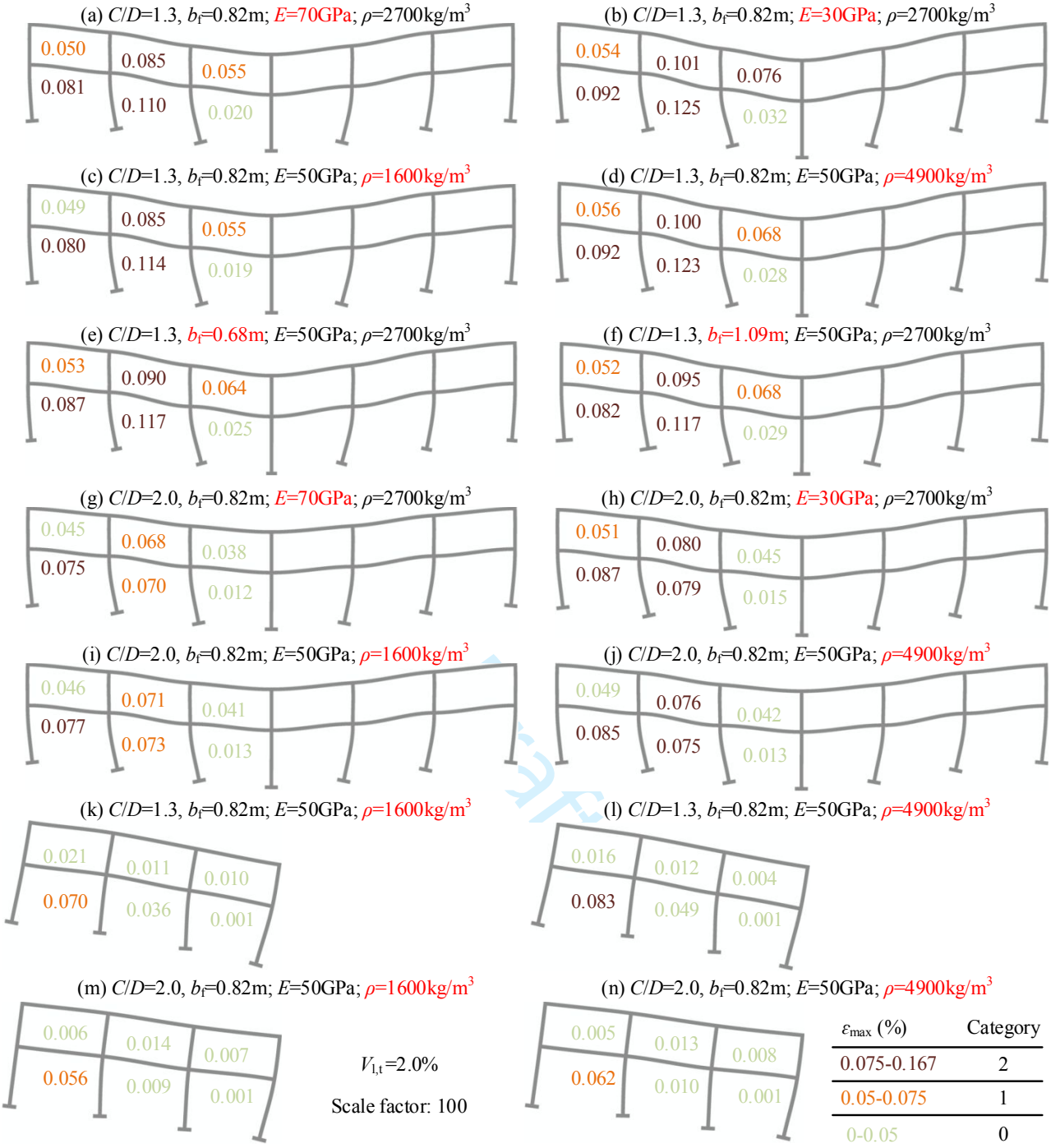

Figure 13. Deformed shape and the values of maximum tensile strain of frames: the effects of building stiffness (a, b), (g, h), foundation pressure (c, d), (i, j), (k, l), (m, n) and footing width (e, f) on structural distortion

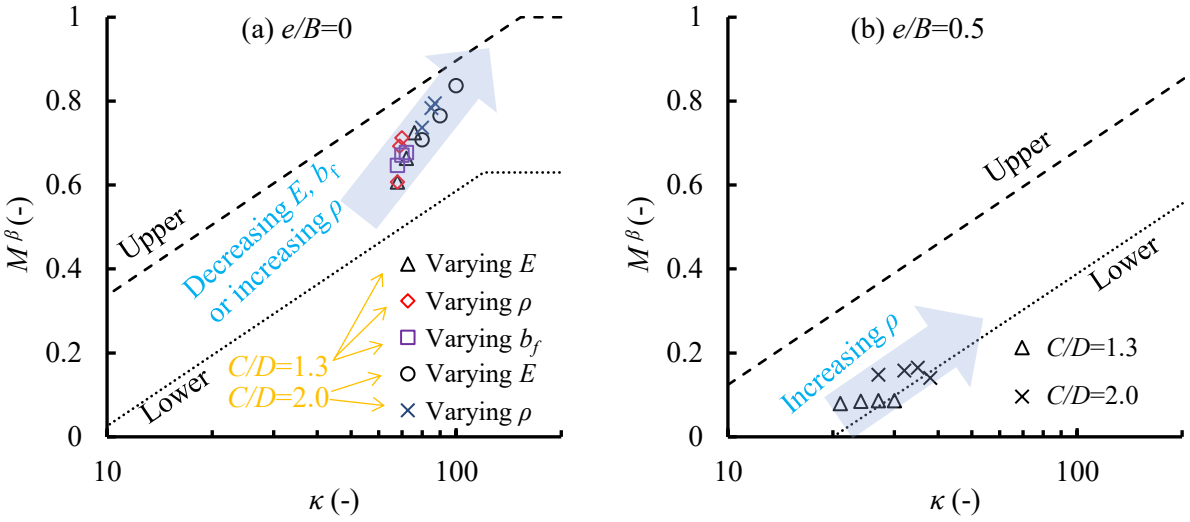

Figure 14. Modification factor of angular distortion against relative stiffness, upper and lower envelopes from Xu et al. (2021b): (a) central buildings; (b) eccentric cases

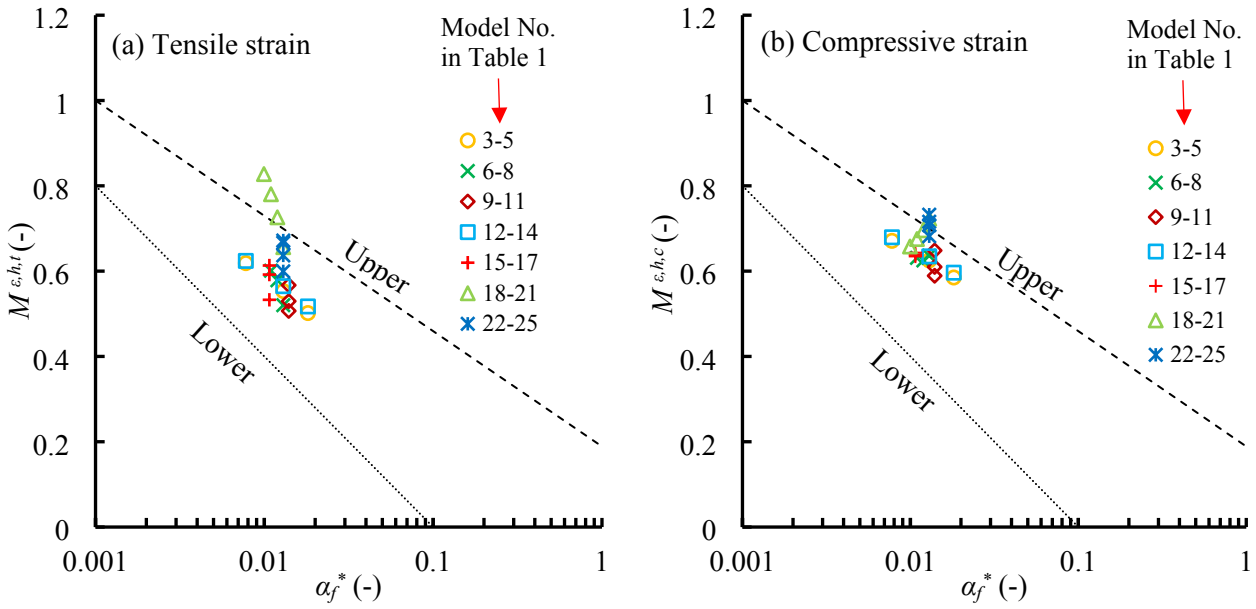

Figure 15. Modification factor of horizontal strain against relative stiffness, upper and lower envelopes from Franza et al. (2017): (a) tensile strain; (b) compressive strain